






# Multiplexing mutation rate assessment: determining pathogenicity of Msh2 variants in *Saccharomyces cerevisiae*

Anja R. Olloidal <sup>1,2</sup>, Chiann-Ling C. Yeh <sup>2</sup>, Aaron W. Miller,<sup>2,†</sup> Brian H. Shirts <sup>3</sup>, Adam S. Gordon <sup>4</sup> and Maitreya J. Dunham <sup>2,\*</sup>

<sup>1</sup>Molecular Cellular Biology Program, University of Washington, Seattle, WA 98195, USA,

<sup>2</sup>Genome Sciences Department, University of Washington, Seattle, WA 98195, USA,

<sup>3</sup>Department of Laboratory Medicine, University of Washington, Seattle, WA 98195, USA, and

<sup>4</sup>Department of Pharmacology, Northwestern University, Chicago, IL 60208, USA

<sup>†</sup>Present address: Zymergen, Emeryville, CA 94608, USA.

\*Corresponding author: Email: maitreya@uw.edu

## Abstract

Despite the fundamental importance of mutation rate as a driving force in evolution and disease risk, common methods to assay mutation rate are time-consuming and tedious. Established methods such as fluctuation tests and mutation accumulation experiments are low-throughput and often require significant optimization to ensure accuracy. We established a new method to determine the mutation rate of many strains simultaneously by tracking mutation events in a chemostat continuous culture device and applying deep sequencing to link mutations to alleles of a DNA-repair gene. We applied this method to assay the mutation rate of hundreds of *Saccharomyces cerevisiae* strains carrying mutations in the gene encoding Msh2, a DNA repair enzyme in the mismatch repair pathway. Loss-of-function mutations in *MSH2* are associated with hereditary nonpolyposis colorectal cancer, an inherited disorder that increases risk for many different cancers. However, the vast majority of *MSH2* variants found in human populations have insufficient evidence to be classified as either pathogenic or benign. We first benchmarked our method against Luria–Delbrück fluctuation tests using a collection of published *MSH2* missense variants. Our pooled screen successfully identified previously characterized nonfunctional alleles as high mutators. We then created an additional 185 human missense variants in the yeast ortholog, including both characterized and uncharacterized alleles curated from ClinVar and other clinical testing data. In a set of alleles of known pathogenicity, our assay recapitulated ClinVar's classification; we then estimated pathogenicity for 157 variants classified as uncertain or conflicting reports of significance. This method is capable of studying the mutation rate of many microbial species and can be applied to problems ranging from the generation of high-fidelity polymerases to measuring the frequency of antibiotic resistance emergence.

**Keywords:** mutation rate; chemostat; MSH2; yeast

## Introduction

Mutation rate is the timer for many different error-prone processes: how many cycles of PCR before the polymerase makes a mistake, how long before the bacterial infection becomes resistant to existing medications, or how quickly DNA damage will result in the uncontrolled growth of a cancerous tumor. An example of the latter is germ line variants in mismatch repair (MMR) pathway genes. These have strong implications for human health and are responsible for the cancer risk syndrome known as hereditary nonpolyposis colorectal cancer (HNPCC) (Lynch *et al.* 2015; Peltomäki 2016). In patients carrying pathogenic alleles, increased surveillance can detect cancers early, improving treatment outcomes (Gupta *et al.* 2019). There are a large number of human MMR variants, and many are classified as variants of uncertain significance (VUS) (Starita *et al.* 2017). Functional data obtained from model organisms can be used to assess potential pathogenicity of these variants (Richards *et al.* 2015;

Gordon *et al.* 2019). As such, urgently needed is a new way to screen variants to determine whether they increase mutation rate, which may contribute to their pathogenicity.

Existing methods for measuring mutation rate are tedious and not scalable for the challenge of functionally testing hundreds or thousands of VUS. Methods to study mutation rate all have their advantages and disadvantages (Foster 2006). In microbial systems, Luria–Delbrück fluctuation tests, mutation accumulation lines, and Novick–Szilard chemostat mutation accumulation experiments are the most widely used (Luria and Delbrück 1943; Lynch *et al.* 2008). These methods currently require initiating populations with single clones, which necessarily limits the ability to multiplex experiments. For mutants in MMR, there are some additional specific methods such as measuring sensitivity to 6-thioguanine or N-methyl-N'-nitro-N-nitrosoguanidine, which correlates with functionality of subunits of the MMR complex including Msh2 and Mlh1 (Drost *et al.* 2013; Houllberghs *et al.* 2017;

Received: March 01, 2021. Accepted: April 02, 2021

© The Author(s) 2021. Published by Oxford University Press on behalf of Genetics Society of America. All rights reserved.

For permissions, please email: journals.permissions@oup.com

Bouvet et al. 2019; Jia et al. 2020). Genome editing methods such as CRISPR-Cas9 provide a convenient way to introduce variants into human cells, where signatures of MMR deficiency can then be tracked (Rath et al. 2019). Another alternative is cell-free systems, which allow for using the human protein in an assay that checks for ability to repair DNA (Drost et al. 2010, 2012, 2019). While this provides an easy way to see all mutations caused by errors in replication, each variant must be expressed and purified separately, and this strategy is not amenable to being pooled. Also, while these systems work well for MMR complex proteins, they do not generalize to mutation rate variability caused by dysfunction in other protein complexes. Computational strategies theoretically could scale to all possible sites in all proteins of interest and have been demonstrated to be good predictors of destabilizing variants (Nielsen et al. 2017; Abildgaard et al. 2019; Stein et al. 2019). However, they still require further validation using lower throughput methods. To address some of these problems, we wanted to generate a new experimental protocol to do multiplexed, direct assessment of mutation rate that was amenable to any molecular pathways for which mutations can be a read out in an easy to culture and genetically tractable organism, *Saccharomyces cerevisiae*.

In addition to ease of use, yeast is a good model system to study effects on MMR because much of the sequence and function of the pathway is conserved between humans and yeast (Boiteux and Jinks-Robertson 2013). Indeed, many discoveries about MMR originate in studies of *S. cerevisiae*, as the MMR complex is more highly conserved with its human orthologs than that of *Escherichia coli* (Strand et al. 1993, 1995). In addition to the general biology of the MMR complex, yeast has been used to determine the mutation rate of MMR alleles using traditional fluctuation assays, mutation accumulation lines, qualitative patch assays, and fluorescence-based assays (Drotschmann et al. 1999; Gammie et al. 2007; Demogines et al. 2008; Lang and Murray 2008; Martinez and Kolodner 2010; Lang et al. 2013; Shor et al. 2019). These assays all test the full functionality of Msh2; however, none of them allow for pooled assessment of many alleles simultaneously. Although medium-throughput assays exist that take advantage of automated liquid-handling systems (Gou et al. 2019), these still require considerable effort if studying the effect on mutation rate of many different alleles and require maintaining clonal populations.

In an effort to overcome scaling problems inherent to other methods for measuring mutation rate, we have developed a chemostat-based assay that utilizes pools of variants to assay hundreds of alleles simultaneously. The chemostat is a continuous culture device that maintains a constant population size over time by diluting out an actively growing culture at the same rate at which it is growing—defined as steady state. Chemostat conditions have a limiting nutrient, the metabolite which is at a level such that the microbe's growth rate is slowed but not stopped. This combination of slower growth rate and stable population size makes this device ideal for studies determining the rate of biological processes. Novick and Szilard pioneered the use of chemostats to determine mutation rate over 70 years ago, and the approach has been used to study microbial mutation rates in many studies since (Novick and Szilard 1950, 1951; Fox 1955, p. 1; Kubitschek and Bendigkeit 1964; Paquin and Adams 1983). The continuous dilution in the chemostat means an increase in the frequency of a neutral mutation is a result of *de novo* mutation, as opposed to other methods, where such an increase could be explained by both *de novo* mutation and exponential growth. If the neutral mutation is also selectable, such as with some types

of drug resistance (e.g., canavanine resistance in yeast), the mutation rate can be calculated by simply tracking the frequency of resistance over time. Combining this very old technique with next-generation sequencing opens up the possibility for high-throughput study of pools of allelic variants. While studies using traditional fluctuation assays have many replicates of mutation frequency—the number of mutants in a population—they tend to only provide one or two estimates mutation rate—the rate of increase of mutation frequency. We wanted a method in which we could provide many mutation rate calculations at once. We applied this new method to study mutation rate differences caused by missense SNP variants in *MSH2*, a gene that is associated with HNPCC. Msh2 is a part of the MMR complex, which in combination with Msh3, Msh6, Mlh1, and Pms2—named Pms1 in *S. cerevisiae*—binds and fixes small mismatches and indels (Boiteux and Jinks-Robertson 2013). Msh2 is an integral part of the recognition complex (Edelbrock et al. 2013). We completed a proof of principle with previously published variants of *MSH2* and found that the pooled assay recapitulated the results of traditional Luria–Delbrück fluctuation tests, qualitative patch assays, and yeast two-hybrid assays (Gammie et al. 2007). We then assayed an additional 185 *MSH2* missense variants curated from ClinVar, a public repository of clinical variant interpretations derived from diagnostic genetic testing. To do so, we recreated these variants in the homologous sites of yeast *MSH2*, barcoded them along with control WT clones, and measured their mutation rates in a pooled format. Of the 28 variants of known pathogenicity, 100% recapitulated the functional consequence implied by previous clinical interpretation. We then examined 157 VUS from ClinVar and identified 50 variants with significantly different mutation rates from WT as measured by our assay. In addition to ClinVar classifications, data were also compared to tumor sequencing in cancer patients (Shirts et al. 2018); of the 25 VUS for which tumor data were available, 64% had clinical findings that were consistent with our functional data. In total, our data set represents ~6000 individual mutation rate calculations. These data taken together show that our new multiplexed mutation rate assay is an accurate and scalable assay to study the mutation rate of many strains in a pooled format.

## Materials and methods

### Growth in the chemostat

For individually inoculated chemostats, 1 ml of overnight culture was inoculated into 230–245 ml of glucose-limited media (calcium chloride 0.1 g/L, sodium chloride 0.1 g/L, magnesium sulfate heptahydrate 0.5 g/L, potassium phosphate monohydrate 1 g/L, ammonium sulfate 5 g/L, glucose 0.8 g/L). Pools were thawed from the freezer and inoculated straight into the chemostat. Cultures were kept at 30°C and allowed 2 days to grow to saturation and the pumps were turned on to a rate of 40 ml/hour or ~five replacement volumes per day. Chemostats were allowed to reach steady state as determined by optical density and later confirmed by stabilization of CFU counts. Samples were then collected starting at ~15 generations. Sampling the nonselective population involved spinning down  $\sim 2 \times 10^8$  cells, as well as plating ~200 cells onto SC-histidine for accurate counts. For each chemostat, to determine the number of canavanine-resistant mutants, sufficient culture to reach an estimated countable number of colonies (~200) was plated onto SC-arginine-serine-histidine + 60 mg/L canavanine to select for loss-of-function (LOF) mutations in *CAN1*. For pools,  $\sim 6 \times 10^8$  cells were

plated, in addition to those used for counts, onto 15 cm SC-histidine + 60 mg/ml canavanine plates and then allowed to grow at 30°C for 3 days at which point they were scraped for downstream analysis.

### Generation of sequencing libraries

For both the nonselective and mutant population, cells were vortexed vigorously with acid washed beads in resuspension buffer for 3 minutes and then put through the Mini-prep Wizard kit. They were then concentrated using the PCR cleanup Wizard kit.

For unbarcoded pools, *MSH2* was amplified from the plasmid vector using 15 rounds of PCR to prevent overamplification. Then Nextera sequencing libraries were generated using the Nextera-Xt kit. The average library size was 500 bp and sequenced using a Nextera 500 with paired end 150 bp reads at a depth of ~30,000 reads over the length of *MSH2*. The run was conducted according to the manufacturer's specifications.

For barcoded pools, PCR amplification of the amplicon containing the barcode was done using 15–22 cycles of PCR using custom Nextera Primers, listed in Supplementary Table S3. A comparison of PCR replicate barcode values is in Supplementary Figure S5. Sufficient amplification was determined by qPCR. The amplicon was purified using dual sided Sepharose bead cleanup to isolate the 250 bp amplicon. Samples were then pooled at equal molar ratios and run on the NextSeq 550 using paired end reads of both 75 or 150 cycles using custom read and index primers (Supplementary Table S3) at a read depth of ~1.7 million reads for the mutant population and 0.5 million reads for the nonselective population. Number of reads roughly corresponded with the number of colonies collected for the mutant pool and 100× coverage of the known number of barcodes for the nonselective population.

### Data analysis of direct sequencing of unbarcoded plasmid pools

Reads were demultiplexed using *bcl2*, allowing for no mismatches in the index read. Reads were then processed first by Trim Galore (Krueger 2019) to remove adaptors, then reads were collapsed using PEAR (Zhang et al. 2014) then aligned to the yeast *MSH2* sequence using BowTie2 (Langmead and Salzberg 2012), a SAM file was generated using Samtools (Li et al. 2009), and then the make up at each base pair was generated using Pysamstats (Miles 2019). Data were manipulated in Excel, and then data points were graphed in R (Supplementary Files S2 and S3) using ggplot (Wickham 2009).

### Data analysis pipeline for barcoded pools

Reads were shortened to the barcode length using a custom python script, fed into PEAR to combine forward and reverse reads, then fed into Enrich (Fowler et al. 2011) to count barcodes. These counts were fed into a custom R script (Supplementary File S2) which manipulated data and plotted using ggplot2. All data required to run the custom R script are in Supplementary File S3, in tabs labeled with the variable names.

### Competition of *msh2Δ* and WT

GFP driven by the *TEF2* promoter was introduced to the *msh2Δ* and *his3Δ* strain by mating. Competitions were set up by individually inoculating 20 ml glucose limited chemostats with 1 ml of saturated culture of each stated strain. The strains were allowed to grow up for 2 days before the pumps were turned on. After reaching steady state after ~10 generations, cultures were mixed half and half, and GFP percentage was monitored twice a

day via flow cytometry. Fitness effects were calculated by taking the slope of the ln of the GFP-tagged to non-GFP-tagged strains over time.

### Making of unbarcoded pools

Plasmid DNA was extracted from *E. coli* strains sent from Alison Gammie (Gammie et al. 2007), pooled, and used to transform YMD4328: FY4 *msh2Δ* and *his3Δ* to ~20× coverage.

### Mapping human variants on the yeast Msh2 protein

Variants in human *MSH2* found in ClinVar were mapped to the yeast *MSH2* sequence.

Putative functional alleles uncovered in humans were adapted for testing in *S. cerevisiae* using a pairwise protein sequence alignment of the two orthologs. The human *MSH2* protein was aligned (NP\_000242.1, uniprot: P43246) with the orthologous *Msh2* in *S. cerevisiae* (strain S288c, uniprot: P25847) using UniProt's Clustal Omega webtool with default parameters (<https://www.uniprot.org/align/>). The pairwise alignment was validated by comparing with similar human-to-yeast missense allele adaptations in the literature (Gammie et al. 2007).

### Generating barcoded variants

Variants containing a homolog within the yeast allele were then ordered as gene products from Twist Biosciences. The gene products were ligated into the pRS413 vector containing the yeast *MSH2* promoter using Gibson and terminator and used to transform DH5α cells at 30X coverage. DNA was extracted using the Mira-Prep protocol (Pronobis et al. 2016) and then digested with *SacI* to linearize. A barcode along with randomized sequence were inserted into the linearized vector using Gibson assembly and then used to transform DH5α cells. Transformants were collected such that there was 5X barcode coverage for each allele. DNA was extracted again using the Mira-prep protocol and digested with *SacI* to linearize any unbarcoded alleles and transformed once more to take advantage of *E. coli*'s inability to be transformed by linear DNA that does not have homology overhangs. Colony PCR was done and 0% of clones contained no barcode and ~6% contained 2–3 barcodes. DNA was once again extracted with the Mira-Prep protocol and then used to transform YMD4328: FY4 *msh2Δ* and *his3Δ flo1Δ* FY4. The *flo1Δ* is present to reduce the prevalence of flocs (Hope et al. 2017). Transformants were collected such that there was 20X coverage of each barcode. These were then pooled for future experiments.

### Fluctuation assay validation

For the chosen validated alleles, the strain construction was the same as the barcoded alleles except the variants were kept separate and no barcode was inserted. Fluctuation assays were performed as described in Lang (2018), Lea and Coulson (1949), and Luria and Delbrück (1943). Briefly, each variant was grown up to saturation in SC-histidine + 2% glucose and then diluted 1:10,000 in either SC-histidine + 2% glucose for WT-like alleles or SC-histidine + 0.1% glucose for null-like alleles. The diluted cells were placed in a 96-well plate—25 μl for null like alleles, 50 μl for WT-like—covered with Breathe-Easy sealing membrane, and allowed to incubate at 30°C for 48 hours, without shaking. Twenty-four wells selected from across the plate were pooled to determine the average total number of cells, and 68 cultures were plated onto SC-arginine-serine-histidine + 60 mg/L canavanine to select for LOF mutations in *CAN1*. The four corner wells were omitted from analysis due to evaporation. Mutation rate

was estimated by using traditional  $P_0$  method (Luria and Delbrück 1943) as well as with the rSalvador package (Zheng 2017) that uses the Lea–Coulson model (Lea and Coulson 1949; Ma et al. 1992). This package was implemented as described in Jiang et al. (2021).

## Pac-bio analysis

Plasmid fragments containing the barcode and variant were isolated from *E. coli* using the Wizard mini-prep kit, amplified using PCR with Kapa-HiFi, and cleaned up by digesting with DpnI and purifying with Ampure beads. Fragments were prepared for PacBio sequencing using the SMRTbell™ Template Prep Kit 1.0 (Pacific Biosciences) and sent to University of Washington PacBio Sequencing Services for sequencing and Sequel II circular consensus sequence (CCS) analysis (Wenger et al. 2019). BAM files of CCS reads were aligned to the plasmid reference using BWA/0.7.13 mem (Li 2013). Reads that were aligned to the reference sequence were piped to a new BAM file with Samtools/1.9 (Li et al. 2009) and analyzed with cigar strings to validate alignments. Barcodes were then extracted and two barcode-variant maps were generated. One file contains all the barcode-variant reads and the other contains the highest quality read for each unique barcode. Errors found in these files were corrected using a multiple sequence alignment (MUSCLE 3.8.31) (Edgar 2004) of reads sharing the same barcode. Final reads were derived from consensus sequences from these alignments. Ambiguous sequences were fixed by aligning sequences to the highest quality reads using the Needleman–Wunsch algorithm (EMBOSS 6.4.0) (Rice et al. 2000).

## Clinical comparisons

Clinical comparisons were made using retrospective data gathered from clinical laboratory databases for testing performed as part of standard clinical care between 2014 and 2019. This retrospective analysis was done under University of Washington IRB 00007284.

## Results

### A new method for multiplex mutation rate assessment

The chemostat is a continuous culture device that matches the growth rate of an organism to the dilution rate, stabilizing population size and environmental conditions throughout an experiment. Many ways to study mutation rate take advantage of drugs for which WT organisms are sensitive but an LOF mutation causes resistance, which makes it straightforward to track mutant frequency (Whelan et al. 1979; Boeke et al. 1987). However, to determine rate, one must know the number of generations that have elapsed since the mutational event, which is difficult in batch culture. Luria–Delbrück fluctuation assays and mutation accumulation lines use different tactics to convert mutational frequency into a mutation rate. In continuous culture, since the population size stays stable, an increase in resistance is not due to an increase in a lineage, as long as certain underlying assumptions are met, as described in the following section. In the assay we have developed, outlined in Figure 1, we can track many lineages in a pooled manner to determine all of their mutation rates at once. We do this by keeping track of *de novo* mutational events on selective media containing a drug, while controlling for any changes in overall population size by monitoring growth on nonselective media.

Next-generation sequencing of the plasmid recovered from both the nonselective and selective media allows us to track the various lineages over time. This assay is amenable to both barcoded and unbarcoded libraries. With unbarcoded libraries,

we use shotgun sequencing of the allele isolated from the plasmid, using the mutation within the gene itself as a way to track the variant over the course of the experiment. In barcoded libraries, the barcode and variant are first linked using long read sequencing, after which amplicon sequencing of just the barcode reveals the frequency of each variant at each time point. Our method is amenable to both types of analysis to make it more generalizable. In both cases, the increase in resistance frequency over time for all lineages can be calculated, giving us their mutation rates.

Our first application of this method utilizes *S. cerevisiae* and focuses on variants of Msh2, a clinically relevant DNA repair enzyme. However, this assay is amenable to the study of any microbial strain that can be cultured inside a chemostat and any molecular pathway where neutral mutations yield a phenotype that can be selected outside the chemostat.

### Conditions required for mutation rate assessment in the chemostat

To accurately measure mutation rate in the chemostat, certain criteria must be satisfied. First, the readout of mutation rate should be neutral in fitness. Second, resistance should accumulate linearly over the assay period indicating no spontaneous nonneutral mutations arose and reached a detectable frequency. Lastly, there should be no inherent fitness effect due to the variants we seek to characterize. Failure to satisfy these criteria invalidates the assay.

To address the first assumption, we used resistance to canavanine as a read out. LOF mutations in CAN1, which encodes an arginine transporter, prevent uptake of the toxic arginine analog canavanine since the transporter is nonfunctional. In our assay, we use the native CAN1 contained within the genome of our transformed strain to select for mutational events. The use of canavanine to select for LOF mutations within CAN1 has been successfully used to assay mutation rate in yeast previously (Paquin and Adams 1983; Lang and Murray 2008). It has a minimal 1.015% fitness benefit under glucose limitation, the conditions used in this study (Gresham et al. 2008).

To determine the timeframe over which we could observe linear accumulation of resistance, we assayed the mutation rate of *msh2Δ* strains containing either WT MSH2 (MSH2) or pRS413 (*msh2Δ*) using the same conditions as future pooled experiments. Previous work has shown complementation by plasmid-borne WT MSH2 and that variants that abrogate activity elevate the mutation rate in yeast (Strand et al. 1993; Drotschmann et al. 1999; Gammie et al. 2007). Chemostats were individually inoculated with MSH2 and *msh2Δ* strains, and samples were plated every 24 hours to determine which timepoints correspond to the range for linear accumulation of Can<sup>R</sup> mutants (Supplementary Figure S1). We found that between ~12 and 50 generations, resistance to canavanine accumulates at rates consistent with previous literature (Table 1) (Gammie et al. 2007; Lang et al. 2013). The observed lag in linear accumulation can be explained by the approach of the population to steady state, the point at which population growth rate and chemostat dilution rate are balanced [reviewed in (Gresham and Dunham 2014)]. After 50 generations, selection on adaptive mutations is likely the cause of the nonlinear increase (Paquin and Adams 1983; Adams et al. 1985). From this, we determined that all future experimental timepoints must be taken between ~12 and 50 generations to accurately determine the mutation rate. If we are to multiplex this assay, null-like *msh2* variants should not have a large fitness effect, otherwise we cannot determine the difference

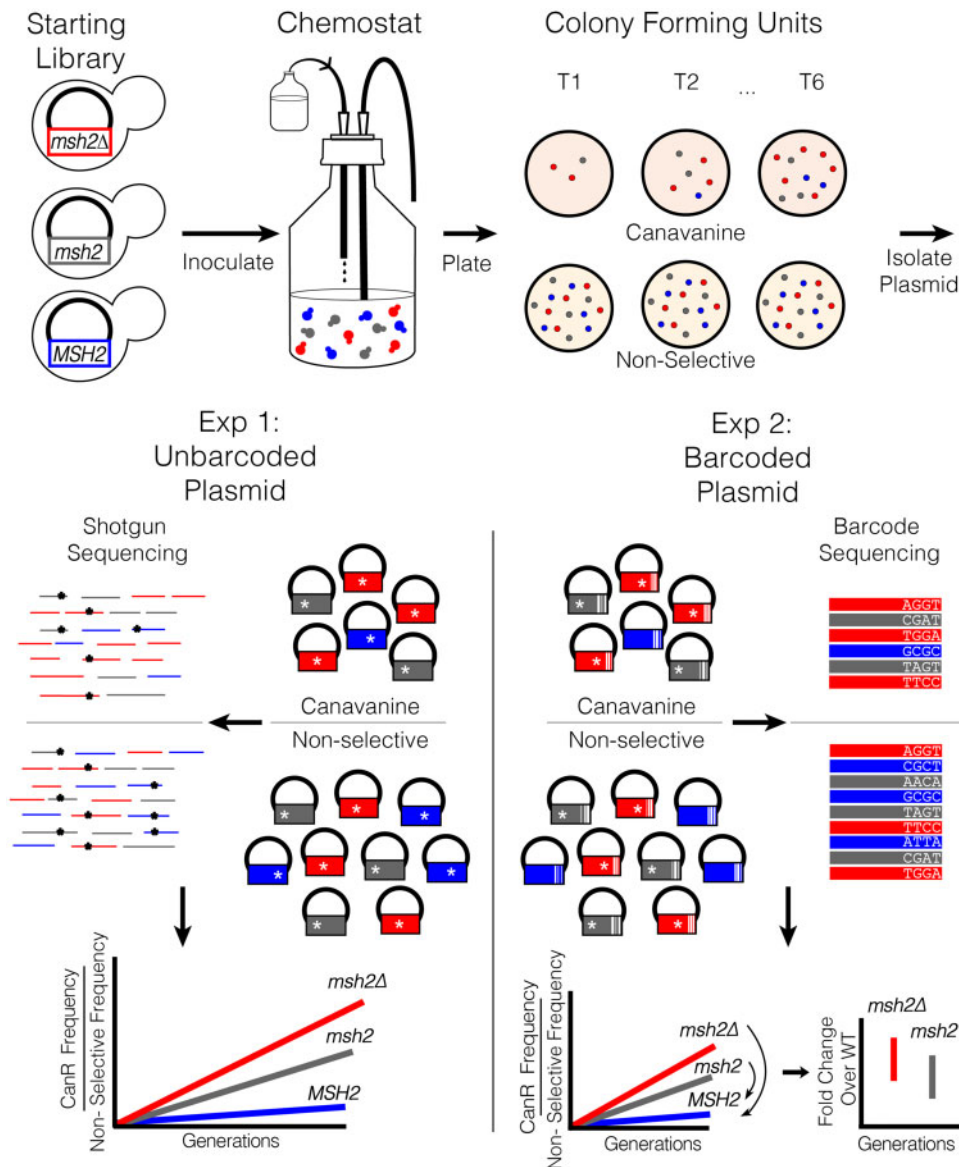


**Figure 1** A schematic outlining the multiplexed mutation rate method. A pool of alleles is inoculated into a chemostat. Samples are plated onto nonselective media or media containing canavanine to select for LOF mutations in *CAN1*. Plasmid is isolated from the canavanine selected plates as well as from the nonselective pool. The assay can handle both unbarcoded and barcoded plasmids using a shotgun or barcode sequencing, respectively. In both cases, the frequency of the allele on selective canavanine media is divided by its presence in the total pool and tracked over time to generate the mutation rate. With barcoded plasmids, barcoded WT can be used to determine the fold change of variants against an internal control.

between a *de novo* mutation and expansion or contraction of a resistant lineage.

In a head-to-head competition between WT and *msh2Δ*, we found a 1.097% fitness defect associated with the *msh2Δ* over the short course of our experiment (Supplementary Figure S1). This means we will likely slightly underestimate mutation rate of high mutators. However, by correcting our mutant frequency by the relative population frequency of each variant, we can mitigate the effects of both the strain manipulation and resistance to canavanine.

### Pools of alleles accumulate mutations at expected rates

Mutation rate can vary even under very similar conditions, and thus multiple replicate assays must be done to obtain accurate measurements. We created a pooled assay to easily increase the

**Table 1** Mutation rates of control pure cultures and pools

| Relevant genotype | CanR rate                       | Fold induction CAN |
|-------------------|---------------------------------|--------------------|
| MSH2              | $1.52 \times 10^{-7} \pm 0.07$  | 1                  |
| <i>msh2Δ</i>      | $49.44 \times 10^{-7} \pm 2.6$  | 29                 |
| Unbarcoded pool   | $21.62 \times 10^{-7} \pm 2.53$ | 13                 |
| Barcoded pool     | $39.6 \times 10^{-7} \pm 2.1$   | 26                 |

<sup>a</sup> Rate, mutations per generation.

number of replicates for each individual mutation rate assessment. We first established a proof of principle assay with 46 previously published alleles of MSH2 (Gammie et al. 2007) (Figure 2, Supplementary Table S1). We transformed the *msh2Δ* strain with a pool of the MSH2 alleles contained within plasmids, inoculated aliquots of the pool into four independent 200 ml chemostats, and from each collected six samples on selective and

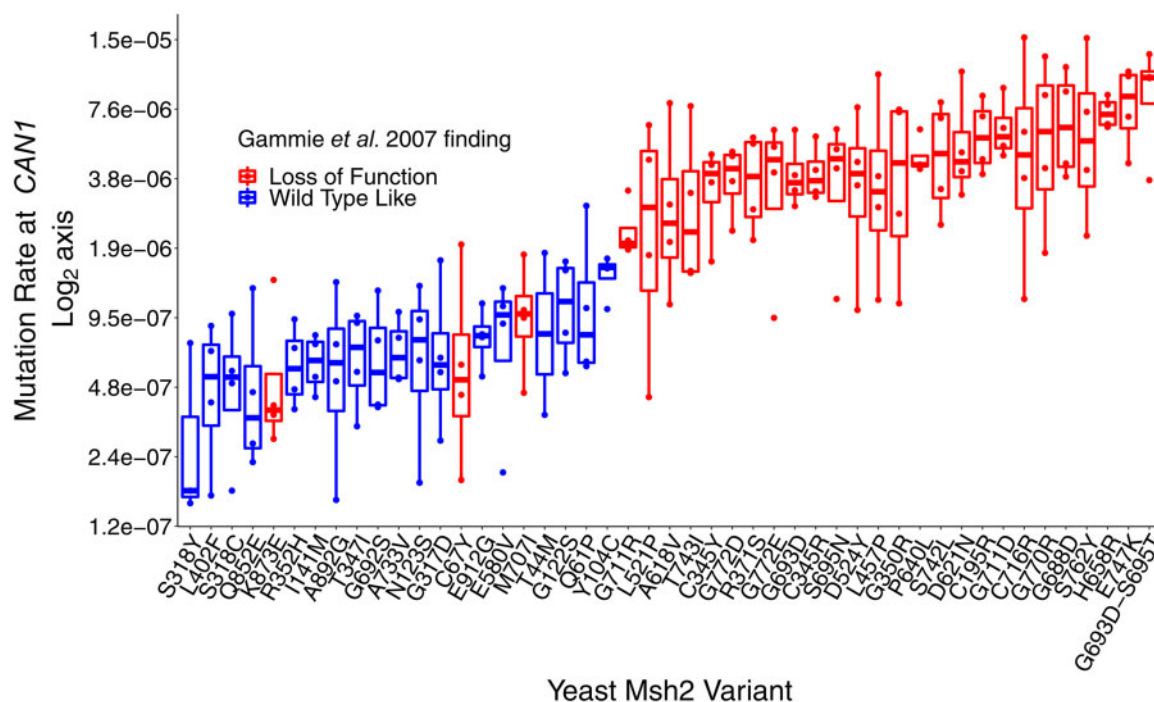


**Figure 2** Calculation of mutation rates of indicated alleles using multiplexed mutation rate assessment. Mutation rate (CanR per generation) of previously studied alleles, colored by the phenotype found in [Gammie et al. 2007](#). Mutation rates are plotted on a  $\log_2$  axis and points represent measurements from separate chemostats.

nonselective media over 50 generations, as determined from the control experiments described above. Plasmid was recovered from all samples, plasmid-borne *MSH2* alleles were amplified by PCR and subjected to shotgun short read sequencing, and the frequency of each allele from the canavanine-resistant pool was normalized by the frequency in the nonselective pool and converted into colony counts (see Materials and methods).

The average mutation rate of this pool is 13X over wild type ([Table 1](#)), which approximates what is expected in a pool containing both LOF and WT-like alleles. In [Figure 2](#), the mutation rates of each allele as measured at *CAN1* are plotted. We compared the results to the phenotype found in previous work using qualitative patch assays, Luria–Delbrück fluctuation tests, and yeast two-hybrid assays between *Msh2* and its subunit partners *Msh3* and *Msh6* ([Figure 2](#), [Supplementary Table S1](#)). With the exception of three alleles (K873E, C67Y, and M707I), alleles previously described as WT-like all grouped together, as did the LOF alleles. C67Y was classified as LOF due to a lack of subunit interaction and a qualitative patch assay in previous work. This lack of subunit interaction may not be reflected in our mutation rate assay and perhaps explains the lack of correspondence to the qualitative measurement. K873E and M707I both showed an LOF phenotype measured at *CAN1* but were found to be WT-like when testing for dinucleotide instability. These alleles exist at the edge of the classification between LOF and WT-like in the compared study and could potentially explain why the results are discordant. These data show a grouping of the high mutators and low mutators, indicating that our new method can largely replicate the results of previous efforts to measure allele-specific effects on mutation rate.

### Simultaneous measurement of mutation rate among 2000 different lineages

To determine the limit on the number of alleles that can be assayed at once, additional alleles of *Msh2* were curated from

the clinical database ClinVar ([Landrum et al. 2014](#)). These human *Msh2* variants were mapped onto the yeast *MSH2* gene; only sites with a residue conserved between both orthologs were considered. Twenty-eight alleles with known pathogenicity were included as well as 216 VUS. Alleles in the Walker A ATPase domain and the linker region, which are more highly conserved between humans and yeast, were given precedence ([Gammie et al. 2007](#)). Alleles were barcoded a median of five times ([Supplementary Figure S7](#)) and the barcode and variant were associated with long-read Pacific Biosciences sequencing. Of the 244 alleles synthesized, 185 variants covered by 1237 barcodes were able to be assayed. In addition, 737 barcodes were associated with WT, giving a robust internal control ([Figure 3A](#)). The 59 variants not assayed were due to low barcode coverage of the variant in the pool, low read coverage during sequencing, or because the barcode lineage showed evidence of a fitness altering mutation ([Supplementary Figures S2, S3, and S6](#)). The number of variants that can be assayed is dependent on the composition of the pool, with higher mutators being easier to assay than lower mutators, results from this pool of *Msh2* variants indicate that the assay is capable of tracking ~2000 barcodes at once.

### Internal WT barcodes can identify differences in mutation rate among alleles

The addition of barcodes, while requiring additional work and cost, can provide internal controls to the pooled mutation rate assay, as each genotype can be tracked in multiple independent lineages. The cumulative mutation rate of the barcoded pool containing novel variants of *Msh2* was  $3.96 \times 10^{-6}$  CanR/generation, a 26-fold increase over WT ([Table 1](#)). The WT barcodes in this assay showed a median mutation rate between  $1.09 \times 10^{-6}$  and  $3.59 \times 10^{-6}$ —approximately 10-fold higher than the expected rate ([Figure 3A](#)). Traditional fluctuation assays completed on a strain

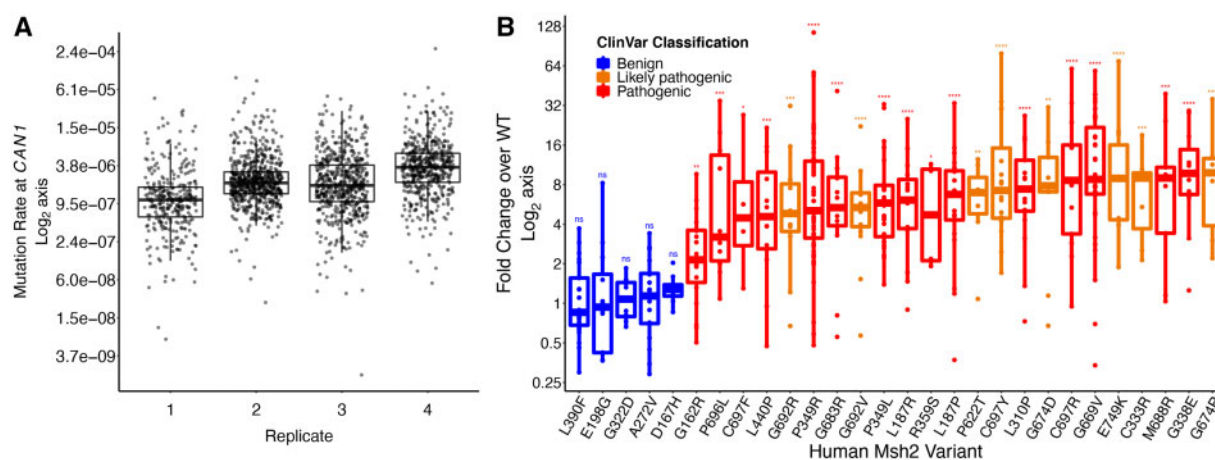


**Figure 3** Control alleles of Msh2 in barcoded experiment pool. (A) Calculated mutation rates (CanR per generation) of WT barcodes in four replicate experiments plotted on a Log<sub>2</sub> axis. (B) Fold change over WT plotted on a Log<sub>2</sub> axis, colored by pathogenicity classification in ClinVar. Points represent individual barcoded measurements from the four replicate experiments. Significance determined by comparing variants to the WT barcodes by a Wilcoxon rank-sum test with the Benjamini–Hochberg correction for multiple hypothesis testing. \* $P < 0.05$ ; \*\* $P < 0.01$ ; \*\*\* $P < 0.001$ ; \*\*\*\* $P < 0.0001$ .

containing the WT plasmid recapitulated individual chemostat assays, indicating that it was not a strain or complementation issue (Supplementary Figure S8). While the source of this global increase in mutation rate is unknown, it can be controlled for by the internal WT barcodes. All variant barcodes in the pool were compared to the internal median WT mutation rate of that pool to calculate fold change over WT for each variant. Inclusion of barcoded WT allows for a robust internal control for mutation rate assessment, which mitigates spurious sources of increased mutation.

### Allele-specific mutation rates recapitulate ClinVar pathogenicity classifications

To determine whether the variants in the barcoded pool recapitulated clinical variant interpretations reported from diagnostic testing, we first looked at variants with known pathogenicity scores in ClinVar. The control variants used have a review status of two or higher, which is a classifier for strong evidence for variant classification in ClinVar (Figure 3B). Variants that shared the same ClinVar classification were found to have similar mutation rates. All five benign variants s “23 out of 23 pathogenic” for correctness.] and likely pathogenic alleles showed a significant increase in mutation rate compared to WT. Due to the limited number of previously characterized variants in the pool, it is difficult to determine true sensitivity and specificity scores; however, these data lend confidence to our ability to bin variants into pathogenic or benign categories. Based on the results of known variants, we have created four bins: variants that do not differ significantly from WT are potentially benign (1). Those with values ranging between 1.3× and 1.4× over WT are likely intermediate (2). Those which are significantly higher than WT are potentially pathogenic (3). The lowest fold change that showed a significant difference from WT was 1.4×, so we classified those which are above this threshold but do not reach significance as possibly pathogenic (4). Traditional fluctuation assays on variants which had heightened mutation rates but did not reach significance recapitulated the higher mutation rate (Supplementary Table S4), lending credence to this possibility pathogenic classification. We were heartened to see our assay recapitulates previous clinical interpretations and that the use of control alleles allowed for the generation of bins to provide information on the VUS assayed.

### Estimating pathogenicity of VUS

We were able to assay 157 SNP VUS in this assay. Of 157 variants, 50 showed a significant difference in mutation rate in comparison to WT and were classified as potentially pathogenic. The mutation rates of these 50 variants are given in Table 2. A summary of the fold changes of all variants is found in Supplementary Table S1. We found that one variant, K449N, had a significantly lower mutation rate than WT, though this result did not replicate in an individual fluctuation assay on this variant (Supplementary Table S4). The mechanism of this possible lowered mutation rate and whether it is a biologically relevant is unknown and could provide an interesting point of study if later confirmed. The 50 VUS that showed a significant increase in mutation rate ranged from 1.39-fold over WT to 13-fold over WT. No alleles assayed had a full LOF phenotype—which would be characterized by a 30-fold increase in mutation rate. This may reflect the dynamic range of the assay or it may reflect that no true LOF alleles existed in the data set. In an attempt to address this, a validation set of nine alleles was subjected to traditional fluctuation assays (Supplementary Table S4). hMSH2 variant R680P recapitulated the 13-fold increase found in the pooled assay—indicating that the upper range of the values found in the assay are correct. For future experiments, it may be wise to include barcoded deletion strains at a low frequency to directly address the dynamic range of the assay. Taken in total, this data set provides evidence of pathogenicity for an additional 157 VUS of MSH2; 83 will be classified as potentially benign, 7 intermediate, 17 possibly pathogenic, and 50 potentially pathogenic. While additional study would be required before these classifications could inform clinical diagnosis, these data represent a first indication of the effects of these mutations on function and could be used as a line of evidence according to American College of Medical Genetics (ACMG) criteria (Richards et al. 2015).

### Associating variant data with clinical and tumor sequencing phenotypes

To more accurately compare clinical data with the outputs of this screen, the fold change calculations were converted to scores. Table 3 contains information on variants that have clinical findings associated with them. Clinical summaries were gathered from data provided to the University of Washington

**Table 2** Mutation rates of significantly different alleles

| Human genotype | Yeast genotype | Count <sup>a</sup> | Fold induction CAN <sup>b</sup> | IQR <sup>c</sup> | Sig <sup>d</sup> |
|----------------|----------------|--------------------|---------------------------------|------------------|------------------|
| K449N          | K466N          | 10                 | 0.56                            | 0.28             | ***              |
| G761R          | G780R          | 31                 | 1.39                            | 0.96             | ***              |
| M672R          | M691R          | 32                 | 1.61                            | 3.37             | ****             |
| R711Q          | R730Q          | 25                 | 1.62                            | 2.63             | ****             |
| P349A          | P361A          | 61                 | 1.79                            | 2.03             | *                |
| V695L          | V714L          | 12                 | 2.08                            | 1.77             | ****             |
| Q681E          | Q700E          | 20                 | 2.09                            | 2.69             | ****             |
| R359K          | R371K          | 7                  | 2.25                            | 1.26             | ****             |
| M672V          | M691V          | 37                 | 2.27                            | 2.37             | **               |
| H783Y          | H802Y          | 11                 | 2.38                            | 1.82             | ****             |
| S676P          | S695P          | 8                  | 2.48                            | 4.55             | *                |
| A609P          | A627P          | 12                 | 2.56                            | 3.36             | **               |
| G761V          | G780V          | 19                 | 2.71                            | 2.82             | ****             |
| A700E          | A719E          | 9                  | 2.78                            | 3.79             | ***              |
| H783D          | H802D          | 7                  | 2.79                            | 4.53             | *                |
| G683E          | G702E          | 54                 | 2.88                            | 3.62             | ****             |
| A689V          | A708V          | 11                 | 3.17                            | 2.58             | ****             |
| P696S          | P715S          | 5                  | 3.27                            | 1.66             | **               |
| R524H          | R542H          | 9                  | 3.49                            | 5.85             | **               |
| R524C          | R542C          | 13                 | 3.61                            | 7.10             | ****             |
| K675E          | K694E          | 8                  | 3.66                            | 7.49             | **               |
| T724M          | T743M          | 34                 | 3.83                            | 3.51             | *                |
| P622Q          | P640Q          | 5                  | 3.95                            | 2.00             | ***              |
| P622A          | P640A          | 9                  | 4.12                            | 3.17             | **               |
| S676L          | S695L          | 5                  | 4.18                            | 1.43             | ***              |
| R524L          | R542L          | 12                 | 4.18                            | 2.22             | ****             |
| Y43D           | Y43D           | 7                  | 4.31                            | 2.16             | **               |
| E643K          | E662K          | 24                 | 4.41                            | 5.92             | **               |
| G669R          | G688R          | 13                 | 4.90                            | 2.62             | ****             |
| C693R          | C712R          | 13                 | 5.00                            | 10.95            | **               |
| T668P          | T687P          | 17                 | 5.03                            | 11.27            | **               |
| G692E          | G711E          | 14                 | 5.04                            | 8.82             | ****             |
| T724R          | T743R          | 18                 | 5.76                            | 6.85             | **               |
| G683W          | G702W          | 18                 | 5.81                            | 6.00             | **               |
| G827R          | G855R          | 34                 | 5.99                            | 8.72             | **               |
| Q690E          | Q709E          | 15                 | 6.03                            | 8.01             | *                |
| A689P          | A708P          | 9                  | 6.27                            | 5.14             | ***              |
| P670R          | P689R          | 6                  | 6.31                            | 6.23             | ****             |
| G692W          | G711W          | 23                 | 6.33                            | 6.60             | *                |
| G669D          | G688D          | 18                 | 6.63                            | 11.83            | *                |
| G827E          | G855E          | 11                 | 6.95                            | 7.11             | ****             |
| T677R          | T696R          | 13                 | 7.41                            | 4.94             | ****             |
| P349S          | P361S          | 47                 | 7.48                            | 8.01             | ****             |
| G338V          | G350V          | 14                 | 7.98                            | 15.14            | ****             |
| G669C          | G688C          | 12                 | 8.08                            | 5.35             | **               |
| R621Q          | R639Q          | 4                  | 8.29                            | 2.07             | ***              |
| N671D          | N690D          | 13                 | 8.61                            | 6.56             | *                |
| R621P          | R639P          | 13                 | 9.28                            | 10.78            | ****             |
| L310R          | L305R          | 14                 | 9.50                            | 13.27            | ****             |
| C693Y          | C712Y          | 4                  | 9.70                            | 3.71             | ****             |
| R680P          | R699P          | 9                  | 13.00                           | 17.19            | ****             |

<sup>a</sup> Count, the number of times a variant was assayed in total.

<sup>b</sup> For stated genotype, mutation rate (mutations per cell division) was calculated and then compared to the WT mutation rate. Barcode and chemostat replicates are combined to calculate median fold change.

<sup>c</sup> Interquartile range of all barcode and chemostat replicates.

<sup>d</sup> Significance is calculated by a Wilcoxon rank-sum test with the Benjamini-Hochberg correction for multiple hypothesis testing. \* < 0.05; \*\* < 0.01; \*\*\* < 0.001; \*\*\*\* < 0.0001.

Genetics and Solid Tumors Laboratory. An assessment of whether the clinical information is consistent or inconsistent with functional scores was provided by a board-certified molecular pathologist with expertise in this area (B.H.S.). Clinical evidence was considered consistent with functional data when both suggested the variant was pathogenic or benign regardless of the strength or significance of the data. There are several types of information on *MSH2* that can be gathered from patients, families,

and tumors (Thompson et al. 2013; Rañola et al. 2018; Shirts et al. 2018; Li et al. 2020). Personal and family history of colorectal or endometrial cancer provide weak evidence of pathogenicity while personal and family history lacking HNPCC-associated cancers provide weak evidence against pathogenicity (Li et al. 2020). Tumor characteristics of microsatellite instability (MSI-H) and loss of Msh2 and Msh6 on immunohistochemistry staining provide moderate evidence supporting pathogenicity (Thompson et al. 2013; Li et al. 2020). Presence of alternative pathogenic variants in *MSH2* or other genes that explain these tumor or other tumor characteristics provides evidence against pathogenicity, while a second somatic pathogenic variant at heterozygous frequency or loss of heterozygosity in tumor provides moderate and strong evidence supporting pathogenicity, respectively (Shirts et al. 2018). Formal strategies for combining each of these types of data with functional data are outside the scope of this effort. Rather we provide relevant clinical summaries with an overall assessment of whether the clinical information is consistent or inconsistent with functional scores. Of the 25 variants identified, 16 (64%) had clinical data that were consistent with functional data, 4 (16%) had clinical data that were inconsistent with functional data, and 5 (20%) had clinical data that were equivocal or fell in the indeterminate functional score range. Some discordance is expected given that functional data are only one component of the ACMG guidelines for clinical variant interpretation; this discordance is consistent with results of past studies seeking to use other clinical criteria to classify variants (Thompson et al. 2013; Shirts et al. 2018; Li et al. 2020).

## Discussion

We developed a new method for high-throughput mutation rate assessment that combines a mid-20th century method to determine mutation rate with 21st-century next-generation sequencing. This allows for the pooling and multiplexing of mutation rate assessment that has not been accomplished before. We were able to complete over 6000 individual mutation rate calculations over ~2000 lineages covering ~200 variants of *MSH2*, a critical component of MMR. Although we included a high frequency of WT sequences, our analysis indicates many of these could be substituted with additional VUS to increase throughput at minimal cost to accuracy. The assay is limited by the canavanine-resistant subpopulation within a 200 ml chemostat, which is dependent on the mutation rates of the lineages in a pool. One could increase the number of variants to be assayed in a single experiment by increasing the volume of the chemostat, though the logistics of expanding the volume beyond the 2L size of available commercial fermenters may be difficult. Another possible modification would be to utilize alternative marker loci that generate selectable mutations at higher rates than the WT *CAN1* sequence. In addition, the inclusion of barcoded null mutants may provide an additional control to better normalize the results to established mutation rates.

In this work, we estimated the pathogenicity of 157 variants of uncertain or conflicting significance derived from clinical testing. These results provide a key piece of information to testing labs seeking to assign pathogenicity to variants for which little other evidence is available. We have found that our results largely match clinical data obtained from tumors (Shirts et al. 2018). These data in combination with a recent deep mutation scan on Msh2 in a human cell line (Jia et al. 2020) will allow for accurate reclassification of uncertain and conflicting variants in this gene. Our data largely recapitulate the results from Jia et al.



**Table 3** Summary of variants with clinical or tumor data

| Human genotype | Score <sup>a</sup> | 95% CI <sup>b</sup> | Sig <sup>c</sup> | ClinVar <sup>d</sup> | Clinical information <sup>e</sup>   | CST <sup>f</sup> |
|----------------|--------------------|---------------------|------------------|----------------------|---|------------------|
| P27L           | -1.06              | 0.87                | ns               | VUS                  | Heterozygous germ line. MSI-H colon cancer with loss of PMS2 by IHC, under age 30 at diagnosis. Also has heterozygous VUS in <i>MLH1</i> .  | Y                |
| K449N          | -0.84              | 0.44                | **               | VUS                  | Heterozygous germ line. Ovarian cancer. No family history of cancer.  | Y                |
| A54S           | -0.11              | 0.34                | ns               | VUS                  | Heterozygous germ line. No personal history of cancer. Family history early onset colorectal cancer and breast cancer.  | Y                |
| A733T          | 0.11               | 0.93                | ns               | VUS                  | Heterozygous germ line. Breast cancer. Family history of colon, ovarian, and brain cancers.   | Y                |
| P616R          | 0.17               | 0.52                | ns               | VUS                  | Heterozygous germ line. MSI-H endometrial tumor with loss of <i>MSH2</i> and <i>MSH6</i> by IHC. Two other clearly pathogenic LOF <i>MSH2</i> mutations identified in the tumor make this less likely to be pathogenic  | Y                |
| Q374R          | 0.20               | 0.42                | ns               | B                    | Heterozygous germ line. MSI-H endometrial tumor with loss of <i>MLH1-MSH2</i> , <i>MSH6</i> , and <i>PMS2</i> by IHC. The tumor had two other clearly pathogenic somatic mutations in <i>MSH2</i> .   | Y                |
| V655I          | 0.21               | 0.38                | ns               | VUS                  | Heterozygous germ line. Colorectal cancer under age 30. No family history of cancer.  | N                |
| W764R          | 0.27               | 0.68                | ns               | VUS                  | Heterozygous germ line. MSI-H colon tumor with loss of <i>MSH2</i> and <i>MSH6</i> by IHC. Evidence of LOH for <i>MSH2</i> variant in tumor.  | N                |
| L599S          | 0.33               | 0.39                | ns               | VUS                  | Heterozygous germ line. Seen in patient with breast cancer and family history of breast and colorectal cancer.  | Y                |
| V78I           | 0.36               | 0.70                | ns               | VUS                  | Heterozygous germ line. MSS ovarian tumor with other pathogenic variants with no LOH for <i>MSH2</i> variant in tumor.  | Y                |
| I770V          | 0.42               | 0.52                | ns               | VUS                  | Heterozygous germ line. Colorectal cancer diagnosed under age 30. Seen with heterozygous germ line VUS in <i>APC</i> gene.  | —                |
| G761R          | 0.47               | 0.38                | *                | VUS                  | Suspected germ line variant in prostate tumor. IHC for <i>MSH2</i> , <i>MSH6</i> equivocal. MSI equivocal. Apparent <i>MSH2</i> LOH in tumor.   | —                |
| H785R          | 0.75               | 0.51                | ns               | VUS                  | Heterozygous germ line. Colorectal cancer diagnosed over age 70.  | —                |
| P349A          | 0.84               | 0.30                | ***              | VUS                  | Homozygous germ line. MSS colorectal cancer. The tumor also had <i>POLE</i> mutation and ultramutator phenotype.  | —                |
| Q681E          | 1.06               | 0.48                | **               | VUS                  | Heterozygous germ line. MSI-H colorectal cancer diagnosed over age 50. Tumor with loss of <i>MLH1</i> and <i>PMS2</i> explained by double somatic <i>MLH1</i> mutation in tumor.  | N                |
| A609P          | 1.36               | 0.73                | **               | VUS                  | Heterozygous germ line. MSI-H colon cancer with loss of <i>MSH2</i> and <i>MSH6</i> by IHC. Under age 50 at diagnosis. Tumor had one somatic pathogenic <i>MSH2</i> mutation seen at heterozygous frequency in the tumor.   | Y                |
| P696S          | 1.71               | 0.98                | *                | VUS                  | Heterozygous germ line. Personal history of pheochromocytoma, family history of renal and brain cancer.   | N                |
| S676L          | 2.06               | 0.70                | **               | VUS                  | Heterozygous germ line. MSI-H colon cancer diagnosed under age 50. Tumor had loss of <i>MSH6</i> by IHC. Seen with <i>MSH2</i> p. G827R somatic mutation listed below.  | Y                |
| C693R          | 2.32               | 0.80                | ****             | LP                   | Somatic mutation in tumor. MSI-H colon tumor with loss of <i>MSH2</i> by IHC. This was seen with another heterozygous pathogenic mutation in <i>MSH2</i> (1760-1 G > A).  | Y                |
| G692V          | 2.42               | 0.58                | ****             | LP                   | Somatic mutation in tumor. MSI-H neuroendocrine tumor with loss of <i>MSH2</i> and <i>MSH6</i> by IHC. Seen in a tumor with a germ line likely pathogenic variant in <i>MSH2</i> (p.L30R) that had loss of heterozygosity.  | —                |
| G827R          | 2.58               | 0.51                | ****             | VUS                  | Somatic mutation in tumor. MSI-H colon cancer diagnosed under age 50. Tumor had loss of <i>MSH6</i> by IHC. Seen with the germ line variant p. S676L listed above.  | Y                |
| G692W          | 2.66               | 0.61                | ****             | VUS                  | Heterozygous germ line. MSI-H endometrial tumor with loss of <i>MSH2</i> and <i>MSH6</i> by IHC. Cancer diagnosed over age 50. Variant reported by another laboratory to segregate with HNPCC in one family. A variant at the same position (p.G692R, NM_000179.2: c.2074 G to C) is classified as likely pathogenic (class 4) by the InSiGHT consortium. | Y                |
| G827E          | 2.80               | 0.63                | ****             | VUS                  | Heterozygous germ line. Pancreatic cancer diagnosed over age 80. Loss of <i>MSH2</i> and <i>MSH6</i> by IHC.  | Y                |
| N671D          | 3.11               | 0.53                | ****             | VUS                  | Heterozygous germ line. Personal history of colon polyps and family history of colon, uterine, and other cancers.   | Y                |
| L310R          | 3.25               | 0.74                | ****             | P                    | Heterozygous germ line. Seen in a family with multiple MSI-H colon cancers that had loss of <i>MSH2</i> . Co-segregation likelihood ratio for pathogenicity in the family was 44:1. See (Tsai et al., 2019) for complete pedigree information.  | Y                |

<sup>a</sup> For stated genotype, variant mutation rate (mutants per generation) was compared to the WT mutation rate. The score represents  $\log_2$ (median fold change).

<sup>b</sup> 95% confidence interval on  $\log_2$ (fold change).

<sup>c</sup> Significance is calculated by a Wilcoxon rank-sum test with the Benjamini-Hochberg correction for multiple hypothesis testing. \* $P < 0.05$ ; \*\* $P < 0.01$ ; \*\*\* $P < 0.001$ ; \*\*\*\* $P < 0.0001$ .

<sup>d</sup> Initial clinical classification as stated in ClinVar. B, benign; LP, likely pathogenic; P, pathogenic; VUS, variant of uncertain significance.

<sup>e</sup> Clinical information collected from UW Laboratory Medicine. MSI-H, microsatellite instability-high; IHC, immunohistochemistry.

<sup>f</sup> CST, consistent, tumor or clinical data is consistent with functional score. Y = Yes, N = No, — = undetermined.

(Supplementary Figure S9). This will provide physicians better guidance on whom to screen for HNPCC and how often.

Our multiplexed assay works for any protein that affects mutation rate. Thus, it can be used to assess mutation rate variation arising from changes in other MMR proteins, as well as in proteins that act in other DNA repair pathways. Assaying variants in the sequence context of the native human cDNA could be possible for genes that complement the orthologous yeast gene knock-out (Vogelsang *et al.* 2009; Kachroo *et al.* 2015); however, our initial attempts to recapitulate the complementation of *mlh1* and *pms1*—the *S. cerevisiae* orthologue of *PMS2*—with human *MLH1* and *PMS2*, other critical MMR genes associated with HNPCC, were unsuccessful. This, however, does not mean that assaying mutation rate of human alleles of DNA repair enzymes is not possible and in fact would be a very interesting line of study. We further note that our assay has additional limitations in replicating human biology: for example, it is not capable of assaying alleles that perturb splicing, RNA stability, or gene regulation, given that these processes are significantly different in yeast vs human cells.

The current set of alleles could also be tested in different genetic backgrounds, such as in the ubiquitin ligase *san1Δ* background (Arlow *et al.* 2013) which could give additional information on the stability of Msh2 variants and could determine the mechanism behind an increased mutation rate for some variants. It could also be done in the background containing deletions or change of function mutations in other proteins in the MMR complex. Both variant library and background are completely mutable in this system.

Our method should be widely applicable and can be used to answer many other questions associated with mutation rate outside of clinical variant interpretation. While this assay is not appropriate for organisms or strains that are not culturable within the chemostat, that still leaves a large set of questions that can be answered. Accurate, multiplexed measurement of mutation rate variation could be used to screen polymerases for increased or decreased fidelity, to screen the yeast deletion collection for knock-outs that increase mutation rate, or to uncover differences in mutation rate among natural variants of yeast. In conclusion, this method is broadly applicable to many different problems in which mutation rate is a factor and can be used to estimate the pathogenicity of clinically relevant DNA repair enzymes.

## Data availability

All sequencing data are available at <https://www.ncbi.nlm.nih.gov/bioproject/PRJNA662579>. Strains and plasmids are available upon request. Supplementary material available at figshare: <https://doi.org/10.25386/genetics.14132609>. Supplementary File S1 contains figures and tables referenced in this text and Supplementary File S2 contains the custom script used in this work. Supplementary File S3 contains strains and plasmids used in this text, tables from Supplementary File S1 in excel format, as well as data sets required to run the custom script in Supplementary File S2.

Supplementary material is available at <https://doi.org/10.25386/genetics.14132609>.

## Acknowledgments

The authors would like to thank Alison Gammie and Mark Rose for the strains used in this work. Josh Cuperus gave guidance on

computational tools used in this project which the authors are grateful for. The authors appreciate Jolie Carlisle's help with plasmid preps and initial attempts to develop this assay in an alternative system. Pengyao Jiang provided the authors with the scripts implementing rSalvador and helpful comments on the manuscript, for which they are thankful. The authors express their sincere gratitude to Jessica Hartmann for design help on figures. The authors would like to thank Bryce Taylor, Pengyao Jiang, Jeet Patel, Meghan Garrett, Amanda Riley, Kurt Berckmueller, and Patrick Nugent for helpful edits on this manuscript.

## Funding

Research reported in this publication was supported by the National Cancer Institute of the National Institutes of Health (NIH) under award T32CA080416 (A.W.M.), by the National Human Genome Research Institute of the NIH under award T32HG00035 (A.R.O. and A.W.M.), National Science Foundation (NSF) Graduate Research Fellowship DGE-1762114 (C.C.Y.), and by the National Institute of General Medical Sciences of the NIH under award P41 GM103533 (M.J.D.). M.J.D. acknowledges prior support as a Rita Allen Foundation Scholar and as a Senior Fellow in the Genetic Networks program at the Canadian Institute for Advanced Research. This material is based in part upon work supported by the NSF under Cooperative Agreement No. DBI-0939454. The research of M.J.D. was supported in part by a Faculty Scholar grant from the Howard Hughes Medical Institute.

## Conflicts of interest

The authors declared no conflicts of interest.

## Literature cited

- Abildgaard AB, Stein A, Nielsen SV, Schultz-Knudsen K, Papaleo E, *et al.* 2019. Computational and cellular studies reveal structural destabilization and degradation of MLH1 variants in Lynch syndrome. Fleishman SJ, Kuriyan J, Fleishman SJ, editors. *eLife*. 8: e49138. doi:10.7554/eLife.49138.
- Adams J, Paquin C, Oeller PW, Lee LW. 1985. Physiological characterization of adaptive clones in evolving populations of the yeast, *Saccharomyces cerevisiae*. *Genetics*. 110:173–185.
- Arlow T, Scott K, Wagenseller A, Gammie A. 2013. Proteasome inhibition rescues clinically significant unstable variants of the mismatch repair protein Msh2. *Proc Natl Acad Sci U S A*. 110: 246–251. doi:10.1073/pnas.1215510110.
- Boeke JD, Trueheart J, Natsoulis G, Fink GR. 1987. 5-Fluoroorotic acid as a selective agent in yeast molecular genetics. *Methods Enzymol*. 154:164–175. doi:10.1016/0076-6879(87)54076-9.
- Boiteux S, Jinks-Robertson S. 2013. DNA repair mechanisms and the bypass of DNA damage in *Saccharomyces cerevisiae*. *Genetics*. 193: 1025–1064. doi:10.1534/genetics.112.145219.
- Bouvet D, Bodo S, Munier A, Guillermin E, Bertrand R, *et al.* 2019. Methylation tolerance-based functional assay to assess variants of unknown significance in the *MLH1* and *MSH2* genes and identify patients with Lynch syndrome. *Gastroenterology*. 157: 421–431. doi:10.1053/j.gastro.2019.03.071.
- Demogines A, Wong A, Aquadro C, Alani E. 2008. Incompatibilities involving yeast mismatch repair genes: a role for genetic modifiers and implications for disease penetrance and variation in genomic mutation rates. Cohen-Fix O, editor. *PLoS Genet*. 4: e1000103. doi:10.1371/journal.pgen.1000103.

- Drost M, Lützen A, van Hees S, Ferreira D, Calléja F, et al. 2013. Genetic screens to identify pathogenic gene variants in the common cancer predisposition Lynch syndrome. *Proc Natl Acad Sci U S A*. 110:9403–9408. doi:10.1073/pnas.1220537110.
- Drost M, Tiersma Y, Thompson BA, Frederiksen JH, Keijzers G, et al. 2019. A functional assay-based procedure to classify mismatch repair gene variants in Lynch syndrome. *Genet Med*. 21:1486–1496. doi:10.1038/s41436-018-0372-2.
- Drost M, Zonneveld JBM, van Dijk L, Morreau H, Tops CM, et al. 2010. A cell-free assay for the functional analysis of variants of the mismatch repair protein MLH1. *Hum Mutat*. 31:247–253. doi:10.1002/humu.21180.
- Drost M, Zonneveld JBM, Hees S, van Rasmussen LJ, Hofstra RMW, et al. 2012. A rapid and cell-free assay to test the activity of lynch syndrome-associated MSH2 and MSH6 missense variants. *Hum Mutat*. 33:488–494. doi:10.1002/humu.22000.
- Drotschmann K, Clark AB, Kunkel TA. 1999. Mutator phenotypes of common polymorphisms and missense mutations in MSH2. *Curr Biol*. 9:907–910. doi:10.1016/S0960-9822(99)80396-0.
- Drotschmann K, Clark AB, Tran HT, Resnick MA, Gordenin DA, et al. 1999. Mutator phenotypes of yeast strains heterozygous for mutations in the MSH2 gene. *Proc Natl Acad Sci U S A*. 96:2970–2975. doi:10.1073/pnas.96.6.2970.
- Edelbrock MA, Kaliyaperumal S, Williams KJ. 2013. Structural, molecular and cellular functions of MSH2 and MSH6 during DNA mismatch repair, damage signaling and other noncanonical activities. *Mutat Res*. 743-744:53–66. doi:10.1016/j.mrfmmm.2012.12.008.
- Edgar RC. 2004. MUSCLE: multiple sequence alignment with high accuracy and high throughput. *Nucleic Acids Res*. 32:1792–1797. doi:10.1093/nar/gkh340.
- Foster PL. 2006. Methods for determining spontaneous mutation rates. *Methods Enzymol*. 409:195–213. doi:10.1016/S0076-6879(05)09012-9.
- Fowler DM, Araya CL, Gerard W, Fields S. 2011. Enrich: software for analysis of protein function by enrichment and depletion of variants. *Bioinformatics*. 27:3430–3431. doi:10.1093/bioinformatics/btr577.
- Fox MS. 1955. Mutation rates of bacteria in steady state populations. *J Gen Physiol*. 39:267–278.
- Gammie AE, Erdeniz N, Beaver J, Devlin B, Nanji A, et al. 2007. Functional characterization of pathogenic human MSH2 missense mutations in *Saccharomyces cerevisiae*. *Genetics*. 177:707–721. doi:10.1534/genetics.107.071084.
- Gordon AS, Rosenthal EA, Carrell DS, Amendola LM, Dorschner MO, et al. 2019. Rates of actionable genetic findings in individuals with colorectal cancer or polyps ascertained from a community medical setting. *Am J Hum Genet*. 105:526–533. doi:10.1016/j.ajhg.2019.07.012.
- Gou L, Bloom JS, Kruglyak L. 2019. The genetic basis of mutation rate variation in yeast. *Genetics*. 211:731–740. doi:10.1534/genetics.118.301609.
- Gresham D, Desai MM, Tucker CM, Jenq HT, Pai DA, Ward A, et al. 2008. The repertoire and dynamics of evolutionary adaptations to controlled nutrient-limited environments in yeast. *PLOS Genet*. 4:e1000303. doi:10.1371/journal.pgen.1000303.
- Gresham D, Dunham MJ. 2014. The enduring utility of continuous culturing in experimental evolution. *Genomics*. 104:399–405. doi:10.1016/j.ygeno.2014.09.015.
- Gupta S, Provenzale D, Llor X, Halverson AL, Grady W, CGC, et al. 2019. NCCN guidelines insights: genetic/familial high-risk assessment: Colorectal, Version 2.2019. *J Natl Compr Canc Netw*. 17:1032–1041. doi:10.6004/jnccn.2019.0044.
- Hope EA, Amorosi CJ, Miller AW, Dang K, Heil CS, et al. 2017. Experimental evolution reveals favored adaptive routes to cell aggregation in yeast. *Genetics*. 206:1153–1167. doi:10.1534/genetics.116.198895.
- Houlliberghs H, Goverde A, Lusseveld J, Dekker M, Bruno MJ, et al. 2017. Suspected Lynch syndrome associated MSH6 variants: a functional assay to determine their pathogenicity. *PLOS Genet*. 13:e1006765. doi:10.1371/journal.pgen.1006765.
- Jia X, Burugula BB, Chen V, Lemons RM, Jayakody S, et al. 2020. Massively parallel functional testing of MSH2 missense variants conferring Lynch syndrome risk. *Am J Hum Genet*. doi:10.1016/j.ajhg.2020.12.003.
- Jiang P, Ollodart AR, Sudhesh V, Herr AJ, Dunham MJ, et al. 2021. A modified fluctuation assay reveals a natural mutator phenotype that drives mutation spectrum variation within *Saccharomyces cerevisiae*. *bioRxiv*. 2021.01.11.425955. doi:10.1101/2021.01.11.425955.
- Kachroo AH, Laurent JM, Yellman CM, Meyer AG, Wilke CO, et al. 2015. Systematic humanization of yeast genes reveals conserved functions and genetic modularity. *Science*. 348:921–925. doi:10.1126/science.aaa0769.
- Krueger F. 2019. A wrapper around Cutadapt and FastQC to consistently apply adapter and quality trimming to FastQ files, with extra functionality for RRBS data: FelixKrueger/TrimGalore. <https://github.com/FelixKrueger/TrimGalore>.
- Kubitschek HE, Bendigkeit HE. 1964. Mutation in continuous cultures. I. Dependence of mutational response upon growth-limiting factors. *Mutat Res Mol Mech Mutagen*. 1:113–120. doi:10.1016/0027-5107(64)90013-2.
- Landrum MJ, Lee JM, Riley GR, Jang W, Rubinstein WS, et al. 2014. ClinVar: public archive of relationships among sequence variation and human phenotype. *Nucleic Acids Res*. 42:D980–D985. doi:10.1093/nar/gkt1113.
- Lang GI. 2018. Measuring mutation rates using the Luria-Delbrück fluctuation assay. In: M Muzi-Falconi, GW Brown, editors. *Genome Instability*, Vol. 1672. New York, NY: Springer New York. p. 21–31. [http://link.springer.com/10.1007/978-1-4939-7306-4\\_3](http://link.springer.com/10.1007/978-1-4939-7306-4_3).
- Lang GI, Murray AW. 2008. Estimating the per-base-pair mutation rate in the yeast *Saccharomyces cerevisiae*. *Genetics*. 178:67–82. doi:10.1534/genetics.107.071506.
- Lang GI, Parsons L, Gammie AE. 2013. Mutation rates, spectra, and genome-wide distribution of spontaneous mutations in mismatch repair deficient yeast. G3 (Bethesda). 3:1453–1465. doi:10.1534/g3.113.006429.
- Langmead B, Salzberg SL. 2012. Fast gapped-read alignment with Bowtie 2. *Nat Methods*. 9:357–359. doi:10.1038/nmeth.1923.
- Lea DE, Coulson CA. 1949. The distribution of the numbers of mutants in bacterial populations. *J Genet*. 49:264–285.
- Li H. 2013. Aligning sequence reads, clone sequences and assembly contigs with BWA-MEM. *ArXiv13033997 Q-Bio*. <http://arxiv.org/abs/1303.3997>.
- Li H, Handsaker B, Wysoker A, Fennell T, Ruan J, et al. 2009. The Sequence Alignment/Map format and SAMtools. *Bioinformatics*. 25:2078–2079. doi:10.1093/bioinformatics/btp352.
- Li S, Qian D, Thompson BA, Gutierrez S, Wu S, et al. 2020. Tumour characteristics provide evidence for germline mismatch repair missense variant pathogenicity. *J Med Genet*. 57:62–69. doi:10.1136/jmedgenet-2019-106096.
- Luria SE, Delbrück M. 1943. Mutations of bacteria from virus sensitivity to virus resistance. *Genetics*. 28:491–511.
- Lynch HT, Snyder CL, Shaw TG, Heinen CD, Hitchins MP. 2015. Milestones of Lynch syndrome: 1895-2015. *Nat Rev Cancer*. 15:181–194. doi:10.1038/nrc3878.
- Lynch M, Sung W, Morris K, Coffey N, Landry CR, et al. 2008. A genome-wide view of the spectrum of spontaneous mutations in

- yeast. *Proc Natl Acad Sci U S A.* 105:9272–9277. doi:10.1073/pnas.0803466105.
- Ma WT, Sandri G. V, Sarkar S. 1992. Analysis of the Luria–Delbrück distribution using discrete convolution powers. *J Appl Probab.* 29: 255–267. doi:10.2307/3214564.
- Martinez SL, Kolodner RD. 2010. Functional analysis of human mismatch repair gene mutations identifies weak alleles and polymorphisms capable of polygenic interactions. *Proc Natl Acad Sci U S A.* 107:5070–5075. doi:10.1073/pnas.1000798107.
- Miles A. 2019. A fast Python and command-line utility for extracting simple statistics against genome positions based on sequence alignments from a SAM or BAM file.: *alimanfoo/pysamstats*. <https://github.com/alimanfoo/pysamstats>.
- Nielsen SV, Stein A, Dinitzen AB, Papaleo E, Tatham MH, et al. 2017. Predicting the impact of Lynch syndrome-causing missense mutations from structural calculations. *PLOS Genet.* 13: e1006739. doi:10.1371/journal.pgen.1006739.
- Novick A, Szilard L. 1950. Experiments with the chemostat on spontaneous mutations of bacteria. *Proc Natl Acad Sci U S A.* 36: 708–719.
- Novick A, Szilard L. 1951. Experiments on spontaneous and chemically induced mutations of bacteria growing in the chemostat. *Cold Spring Harb Symp Quant Biol.* 16:337–343. doi:10.1101/SQB.1951.016.01.025.
- Paquin C, Adams J. 1983. Frequency of fixation of adaptive mutations is higher in evolving diploid than haploid yeast populations. *Nature.* 302:495–500. doi:10.1038/302495a0.
- Peltomäki P. 2016. Update on Lynch syndrome genomics. *Fam Cancer.* 15:385–393. doi:10.1007/s10689-016-9882-8.
- Pronobis MI, Deutch N, Peifer M. 2016. The Miraprep: a Protocol that uses a Miniprep Kit and provides Maxiprep yields. *PLOS One.* 11: e0160509. doi:10.1371/journal.pone.0160509.
- Rañola JMO, Liu Q, Rosenthal EA, Shirts BH. 2018. A comparison of cosegregation analysis methods for the clinical setting. *Fam Cancer.* 17:295–302. doi:10.1007/s10689-017-0017-7.
- Rath A, Mishra A, Ferreira VD, Hu C, Omerza G, et al. 2019. Functional interrogation of Lynch syndrome-associated MSH2 missense variants via CRISPR-Cas9 gene editing in human embryonic stem cells. *Hum Mutat.* 40:2044–2056. doi:10.1002/humu.23848.
- Rice P, Longden I, Bleasby A. 2000. EMBOSS: the European Molecular Biology Open Software Suite. *Trends Genet.* 16:276–277. doi:10.1016/S0168-9525(00)02024-2.
- Richards S, Aziz N, Bale S, Bick D, Das S, ACMG Laboratory Quality Assurance Committee, et al. 2015. Standards and guidelines for the interpretation of sequence variants: a joint consensus recommendation of the American College of Medical Genetics and Genomics and the Association for Molecular Pathology. *Genet Med.* 17:405–423. doi:10.1038/gim.2015.30.
- Shirts BH, Konnick EQ, Upham S, Walsh T, Ranola JMO, et al. 2018. Using somatic mutations from tumors to classify variants in mismatch repair genes. *Am J Hum Genet.* 103:19–29. doi:10.1016/j.ajhg.2018.05.001.
- Shor E, Schuyler J, Perlin DS. 2019. A novel, drug resistance-independent, fluorescence-based approach to measure mutation rates in microbial pathogens. *mBio.* 10:doi:10.1128/mBio.00120-19.
- Starita LM, Ahituv N, Dunham MJ, Kitzman JO, Roth FP, et al. 2017. Variant interpretation: functional assays to the rescue. *Am J Hum Genet.* 101:315–325. doi:10.1016/j.ajhg.2017.07.014.
- Stein A, Fowler DM, Hartmann-Petersen R, Lindorff-Larsen K. 2019. Biophysical and mechanistic models for disease-causing protein variants. *Trends Biochem Sci.* 44:575–588. doi:10.1016/j.tibs.2019.01.003.
- Strand M, Earley MC, Crouse GF, Petes TD. 1995. Mutations in the MSH3 gene preferentially lead to deletions within tracts of simple repetitive DNA in *Saccharomyces cerevisiae*. *Proc Natl Acad Sci U S A.* 92:10418–10421. doi:10.1073/pnas.92.22.10418.
- Strand M, Prolla TA, Liskay RM, Petes TD. 1993. Destabilization of tracts of simple repetitive DNA in yeast by mutations affecting DNA mismatch repair. *Nature.* 365:274–276. doi:10.1038/365274a0.
- Thompson BA, Goldgar DE, Paterson C, Clendenning M, Walters R, Colon Cancer Family Registry, et al. 2013. A multifactorial likelihood model for MMR gene variant classification incorporating probabilities based on sequence bioinformatics and tumor characteristics: a report from the Colon Cancer Family Registry. *Hum Mutat.* 34:200–209. doi:10.1002/humu.22213.
- Tsai GJ, Rañola JMO, Smith C, Garrett LT, Bergquist T, et al. 2019. Outcomes of 92 patient-driven family studies for reclassification of variants of uncertain significance. *Genet Med.* 21:1435–1442. doi:10.1038/s41436-018-0335-7.
- Vogelsang M, Comino A, Zupanec N, Hudler P, Komel R. 2009. Assessing pathogenicity of MLH1 variants by co-expression of human MLH1 and PMS2 genes in yeast. *BMC Cancer.* 9:382. doi:10.1186/1471-2407-9-382. <http://bmccancer.biomedcentral.com/articles/10.1186/1471-2407-9-382>.
- Wenger AM, Peluso P, Rowell WJ, Chang P-C, Hall RJ, et al. 2019. Accurate circular consensus long-read sequencing improves variant detection and assembly of a human genome. *Nat Biotechnol.* 37:1155–1162. doi:10.1038/s41587-019-0217-9.
- Whelan WL, Gocke E, Manney TR. 1979. The CAN1 Locus of *Saccharomyces cerevisiae*: fine-structure analysis and forward mutation rates. *Genetics.* 91:35–51.
- Wickham H. 2009. ggplot2: Elegant Graphics for Data Analysis. New York: Springer-Verlag (Use R!). <https://www.springer.com/gp/book/9780387981413>.
- Zhang J, Kobert K, Flouri T, Stamatakis A. 2014. PEAR: a fast and accurate Illumina Paired-End reAd mergeR. *Bioinformatics.* 30: 614–620. doi:10.1093/bioinformatics/btt593.
- Zheng Q. 2017. rSalvador: an R package for the fluctuation experiment. *G3 (Bethesda).* 7:3849–3856. doi:10.1534/g3.117.300120.

Communicating editor: J. Surtees